

Bioimage informatics

Bayesian network–response regression

Lu Wang^{1,*}, Daniele Durante², Rex E. Jung³ and David B. Dunson¹

¹Department of Statistical Science, Duke University, Durham, NC 27708, USA, ²Department of Statistical Sciences, University of Padova, Padova 35121, Italy and ³Department of Psychology, University of New Mexico, Albuquerque, NM 87131, USA

*To whom correspondence should be addressed.

Associate Editor: Robert Murphy

Received on August 24, 2016; revised on November 24, 2016; editorial decision on January 15, 2017; accepted on January 28, 2017

Abstract

Motivation: There is increasing interest in learning how human brain networks vary as a function of a continuous trait, but flexible and efficient procedures to accomplish this goal are limited. We develop a Bayesian semiparametric model, which combines low-rank factorizations and flexible Gaussian process priors to learn changes in the conditional expectation of a network-valued random variable across the values of a continuous predictor, while including subject-specific random effects.

Results: The formulation leads to a general framework for inference on changes in brain network structures across human traits, facilitating borrowing of information and coherently characterizing uncertainty. We provide an efficient Gibbs sampler for posterior computation along with simple procedures for inference, prediction and goodness-of-fit assessments. The model is applied to learn how human brain networks vary across individuals with different intelligence scores. Results provide interesting insights on the association between intelligence and brain connectivity, while demonstrating good predictive performance.

Availability and Implementation: Source code implemented in R and data are available at <https://github.com/wangronglu/BNRR>

Contact: rl.wang@duke.edu

Supplementary information: [Supplementary data](#) are available at *Bioinformatics* online.

1 Introduction

We are motivated by recent advances in neuroimaging of structural interconnections among anatomical regions in the human brain. Our focus is on learning how brain structural connectivity networks—also known as connectomes—vary across individuals, and the extent to which such variability is associated with differences in human cognitive traits.

In our application, brain networks are estimated exploiting structural magnetic resonance imaging and diffusion tensor imaging to obtain a $V \times V$ symmetric adjacency matrix A_i for each subject $i = 1, \dots, n$. Each cell $[vu]$ in the matrix corresponds to a pair of brain regions, with $A_{i[vu]} = A_{i[uv]} = 1$ if there are fibers connecting brain regions v and u in subject i , and $A_{i[vu]} = A_{i[uv]} = 0$ otherwise. There are $V = 68$ regions in our study (Desikan *et al.*, 2006) equally

divided in the left and right hemisphere. Refer to Figure 1 for an example of the available data.

There has been an increasing focus on using brain imaging technologies to better understand the neural pathways underlying human traits, ranging from personality to cognitive abilities and mental disorders (Stam, 2014). Our aim is to develop flexible procedures to improve understanding of how the brain structural connectivity architecture varies in relation to a trait of interest $x_i \in \mathbb{R}$ measured for each subject $i = 1, \dots, n$. In our application this trait represents a measure of intelligence available via the FSIQ (Full Scale Intelligence Quotient) score (Jung and Haier, 2007).

Network data are challenging to analyze because they require not only dimensionality reduction procedures to effectively deal with the large number of pairwise relationships, but also flexible formulations

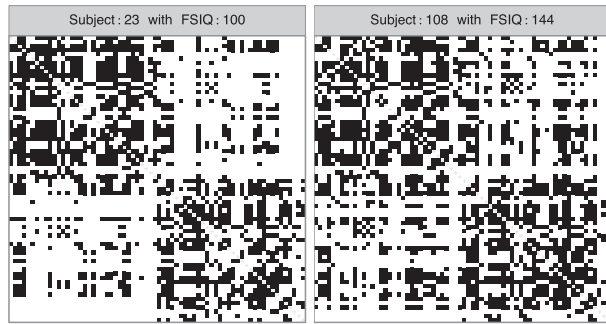


Fig. 1. Binary adjacency matrices for two selected subjects. Black cells denote presence of a connection. White cells denote no connection. FSIQ is an IQ score

to account for the topological structures of the network. Current literature addresses these goals only for a single network observation. Notable examples include exponential random graph models (e.g. Frank and Strauss, 1986), and factorizations covering stochastic block models (Nowicki and Snijders, 2001), mixed membership stochastic block models (Airoldi et al., 2008) and latent space models (Hoff et al., 2002). These procedures reduce dimensionality, incorporate network properties and have been generalized to accommodate regression settings in which there are response variables and network-specific predictors associated with every node $v = 1, \dots, V$ in a single network (e.g. Hochberg et al., 2007; O'Malley and Marsden, 2008). This type of network regression is fundamentally different than our interest in relating a network A_i specific to individual i to a corresponding predictor x_i , for $i = 1, \dots, n$.

In relating the network A_i to a specific trait x_i , a common strategy in neuroscience is to estimate a separate logistic regression for each pair of brain regions to learn changes in their connectivity with the predictor. However, as discussed in Simpson et al. (2013), such massive univariate edge-based studies do not incorporate dependence in connectivity patterns, and therefore ignore relevant wiring mechanisms in the brain architecture. This has motivated an increasing interest in how topological characteristics of a complex network change as a function of a trait (e.g. Rubinov and Sporns, 2010). Typical procedures address this aim by computing a set of summary measures for each network—e.g. network density, transitivity, average path length, assortativity—and enter these statistics as responses in a regression model (e.g. van den Heuvel et al., 2009; Wu et al., 2013). However, reducing the rich network data to a subset of summary measures can discard important information about the brain connectivity and underestimate its changes across the trait.

With these issues in mind, we develop a network–response regression model, which considers the brain network A_i as an object-type response variable having conditional expectation changing flexibly with x_i . To our knowledge, there is no literature addressing this problem, though there are a rich variety of methods for characterizing dynamic changes in a time-specific network A_t , with Holland and Leinhardt (1977), Xing et al. (2010) and Sewell and Chen (2015) considering discrete equally-spaced times and Durante and Dunson (2014) providing a continuous-time formulation. Although the later article provides a useful building block, the time-series setting is fundamentally different from the regression case we consider, motivating careful modifications to incorporate subject-specific variability and other relevant structure.

There is an increasing availability of data motivating network–response regression models. We propose a Bayesian semiparametric formulation that reduces dimensionality and efficiently exploits

network information via a flexible latent space representation, with the latent coordinates of the brain regions varying both systematically—according to a trait of the individual, such as FSIQ—and randomly—due to unobserved traits or measurement errors—across individuals. This formulation allows coherent inference at different scales, including global changes in network topological structures and local variations in edge probabilities.

The paper is organized as follows. In Section 2 we focus on model formulation, prior specification and posterior computation. A simulation study is examined in Section 3. In Section 4 our model is applied to learn changes in the brain network with the FSIQ score, showing improved performance in inference, edge prediction and uncertainty quantification.

2 Materials and methods

Let A_i denote the binary adjacency matrix characterizing the undirected brain network with no self-relationships for the subject i , and x_i the corresponding trait value, for every $i = 1, \dots, n$. As self-relationships are not of interest and A_i is symmetric, we model A_1, \dots, A_n by defining a probabilistic generative mechanism for the vectors $\mathcal{L}(A_1), \dots, \mathcal{L}(A_n)$, with $\mathcal{L}(A_i) = (A_{i[21]}, A_{i[31]}, \dots, A_{i[V1]}, A_{i[32]}, \dots, A_{i[V(V-1)]})^\top$ the vector encoding the lower triangular elements of A_i , which uniquely characterize A_i . Hence, $\mathcal{L}(A_i)$ is a vector of binary elements $\mathcal{L}(A_i)_l \in \{0, 1\}$, $l = 1, \dots, V(V-1)/2$, encoding the absence or presence of an edge among the l th pair of brain regions in subject i .

Based on our notation, developing a regression model for a network-valued response translates into statistical modeling of how a vector of binary data changes across the values of a trait of interest. However, it is important to explicitly incorporate the network structure of our data. In fact, networks are potentially characterized by specific underlying topological patterns which induce dependence among the edges within each brain. As a result, by carefully accommodating the network structure in modeling of $\mathcal{L}(A_1), \dots, \mathcal{L}(A_n)$, one might efficiently borrow information within each $\mathcal{L}(A_i)$ and across the trait x_i , while reducing dimensionality and inferring specific network properties along with their changes across x_i .

2.1 Model formulation

In modeling of $\mathcal{L}(A_1), \dots, \mathcal{L}(A_n)$ we look for a representation which can flexibly characterize variability across individuals in brain connectivity, while accommodating network structure within each brain and learning changes with the trait x_i . Individual variability (e.g. Mueller et al., 2013) and specific network structures (e.g. Bullmore and Sporns, 2009) have been shown to substantially affect the functioning of networked brain systems, with these systems often varying with human traits (e.g. Stam, 2014).

Consistent with the above goals and letting $\mathcal{L}(A_i)$ denote the random variable associated with the brain network of subject i , we characterize individual variability by assuming the edges among pairs of brain regions are conditionally independent Bernoulli variables, given a subject-specific edge probability vector $\pi^{(i)} = \{\pi_1^{(i)}, \dots, \pi_{V(V-1)/2}^{(i)}\}^\top$,

$$\mathcal{L}(A_i)_l | \pi_l^{(i)} \sim \text{Bern}\{\pi_l^{(i)}\}, \quad \pi_l^{(i)} = \text{pr}\{\mathcal{L}(A_i)_l = 1\}, \quad (1)$$

independently for each pair $l = 1, \dots, V(V-1)/2$ and $i = 1, \dots, n$. Equation (1) incorporates individual variability, but fails to account for two key sources of information in our data. In fact, we expect dependence between the edge probabilities in each $\pi^{(i)}$ due to the

network topology. Moreover, it is reasonable to expect that subjects with similar traits will have comparable brain networks. To incorporate these structures, we define the edge probabilities as a function of subject-specific node positions in a latent space, with these positions centered on a higher-level mean which changes with x_i . Specifically, letting l denote the pair of brain regions v and u , $v > u$, we first borrow information within each $\pi^{(i)}$ by defining

$$\text{logit}\{\pi_l^{(i)}\} = Z_l + \sum_{r=1}^R Y_{vr}^{(i)} Y_{ur}^{(i)}, \quad (2)$$

for each $l = 1, \dots, V(V-1)/2$ and $i = 1, \dots, n$. In (2), $Z_l \in \mathbb{R}$ is a similarity measure for the l th pair of regions shared among all individuals, whereas $Y_{vr}^{(i)} \in \mathbb{R}$ and $Y_{ur}^{(i)} \in \mathbb{R}$ denote the r th coordinate of the brain regions v and u for subject i , respectively. This construction has also an intuitive interpretation. In fact, $Y_{vr}^{(i)}$ may measure the propensity of brain region v towards the r th cognitive function in subject i . According to (2), if regions v and u have propensities in the same direction, they will have a high chance $\pi_l^{(i)}$ to be connected. Moreover, embedding the brain regions in a lower-dimensional space via (2) allows dimensionality reduction, and can accommodate several topological properties (Hoff, 2008).

2.2 Prior specification

To conclude our Bayesian specification, we choose priors for the shared parameters Z_l , $l = 1, \dots, V(V-1)/2$, and the subject-specific latent coordinates $Y_{vr}^{(i)}$ for each $v = 1, \dots, V$, $r = 1, \dots, R$ and $i = 1, \dots, n$. These priors are defined to facilitate simple posterior computation, favor borrowing of information between different individuals and allow the latent coordinates to smoothly change across the values of the predictor. Subjects with similar traits are expected to have comparable brain networks. We incorporate this structure by centering the prior for the subject-specific latent coordinates on a higher-level mean smoothly changing with the trait of interest. Then, by updating this prior with the likelihood provided by the data we expect the posterior to flexibly account for possible deviations from prior assumptions, including allowance for uninformative traits.

Consistent with the above considerations, we let

$$Z_l \sim N(\mu_z, \sigma_z^2), \quad (3)$$

independently for $l=1, \dots, V(V-1)/2$; and

$$Y_{vr}^{(i)} \sim N\{\mu_{vr}(x_i), 1\}, \quad (4)$$

independently for every $v = 1, \dots, V$, $r = 1, \dots, R$ and $i = 1, \dots, n$. We set the prior variance of $Y_{vr}^{(i)}$ at 1 because we observed indistinguishable results when replacing (4) with a Student- t distribution. Hence we maintain the Gaussian prior (4) to keep the model parsimonious and computationally tractable. To accommodate systematic deviations, we incorporate mean functions $\mu_{vr}(\cdot)$ characterizing changes in the r th latent coordinate of the v th brain region with the trait of interest.

In modeling $\mu_{vr}(\cdot)$, we could consider a Gaussian process (GP) prior for each $v = 1, \dots, V$ and $r = 1, \dots, R$. However, as the number of nodes increases, we face scalability issues. To reduce dimensionality, we define each $\mu_{vr}(\cdot)$ as a linear combination of a smaller number of dictionary functions $W_{kr}(\cdot)$, $k = 1, \dots, K < V$ and $r = 1, \dots, R$,

$$\mu_{vr}(\cdot) = \sum_{k=1}^K G_{vk} W_{kr}(\cdot), \quad (5)$$

for each $v = 1, \dots, V$ and $r = 1, \dots, R$, where G_{vk} , for $v = 1, \dots, V$ and $k = 1, \dots, K$, are coefficients common to all the subjects. Factorization (5) further reduces the number of unknown functions from $V \times R$ to $K \times R$, where K is typically smaller than V . Factorizations (2) and (5) are not unique; however, we avoid identifiability constraints as the focus of our inference is not on latent coordinates but on how the overall network structure varies systematically with traits and randomly across individuals. Such inferences can be accomplished via appropriate functionals of the edge probabilities in $\pi^{(i)}$, as we will illustrate.

In choosing priors for the components in factorization (5), we first let

$$W_{kr}(\cdot) \sim \text{GP}(0, c) \quad (6)$$

independently for each $k = 1, \dots, K$ and $r = 1, \dots, R$, with c the squared exponential correlation function $c(x_i, x_j) = \exp\{-\kappa(x_i - x_j)^2\}$, $\kappa > 0$. To allow adaptive deletion of unnecessary dictionary functions, we incorporate a shrinkage effect in the prior for the coefficients G_{vk} , $v = 1, \dots, V$ and $k = 1, \dots, K$, letting

$$G_{vk} \sim N(0, \tau_k^{-1}), \quad v = 1, \dots, V, k = 1, \dots, K, \quad (7)$$

$$\tau_k \sim \text{Ga}\{aq^{3(k-1)}, q^{2(k-1)}\}, \quad q > 1. \quad (8)$$

In (7), τ_k provides a global column-wise shrinkage effect on G_{vk} . High values of τ_k force the prior for G_{vk} to be concentrated around zero *a priori*, deleting the effect of the corresponding dictionary function $W_{kr}(\cdot)$ in factorization (5). Equation (8) is carefully defined to allow this shrinkage effect to be increasingly strong as k grows. A graphical representation of our hierarchical model formulation is provided in Figure 2.

2.3 Posterior computation

Given priors defined in equations (3)–(8), posterior computation for model (1) with subject-specific edge probabilities factorized as in (2), proceeds via a simple Gibbs sampler leveraging Pólya-Gamma data augmentation (Polson *et al.*, 2013), which allows conjugate inference in Bayesian logistic regression. We summarize below the main steps of the MCMC routine. Step-by-step derivations are provided in the Supplementary Material.

- Update each augmented data $\omega_l^{(i)}$, $l = 1, \dots, V(V-1)/2$, $i = 1, \dots, n$, from its full conditional Pólya-Gamma distribution.
- Given the data $\{\mathcal{L}(A_i), x_i\}$, $i = 1, \dots, n$, the latent coordinates' matrix $Y^{(i)}$, $i = 1, \dots, n$, and the Pólya-Gamma augmented data $\omega_l^{(i)}$, $l = 1, \dots, V(V-1)/2$, $i = 1, \dots, n$, the full conditionals for Z_l , $l = 1, \dots, V(V-1)/2$ are Gaussian distributions.
- In updating the subject-specific coordinates' matrix $Y^{(i)}$, for each $i = 1, \dots, n$, we block sample the rows of $Y^{(i)}$ in turn conditionally on the rest of the matrix and the parameters G_{vk} , $v = 1, \dots, V$, $k = 1, \dots, K$, $W_{kr}(x_i)$, $k = 1, \dots, K$, $r = 1, \dots, R$. This approach allows rewriting the model (1)–(2) as a Bayesian

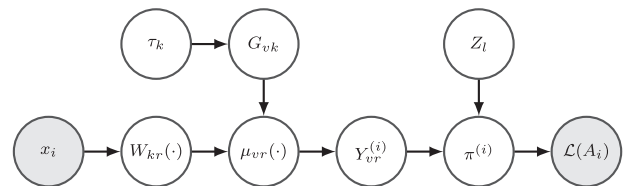


Fig. 2. Graphical representation of our Bayesian network–response regression model

logistic regression for which the Pólya-Gamma data augmentation scheme guarantees conjugate Gaussian full conditionals.

- Given the coordinates' matrix $Y^{(i)}$, $i = 1, \dots, n$ and the traits x_i , $i = 1, \dots, n$, updating for the parameters G_{vk} , $v = 1, \dots, V$, $k = 1, \dots, K$ and the trajectories $W_{kr}(\cdot)$, $k = 1, \dots, K$, $r = 1, \dots, R$ at the observed trait values, proceed by exploiting the properties of GP priors and standard steps in Bayesian linear regression. Since the data are observed for a finite number of subjects, this step uses the multivariate Gaussian representation of the GP. However it is worth noticing that our model is inherently semi-parametric as the GP in (6) induces a prior on the infinite-dimensional space of smooth functions.
- Conditioned on G_{vk} , $v = 1, \dots, V$, $k = 1, \dots, K$, the shrinkage parameters τ_k , $k = 1, \dots, K$ are updated from their full conditional Gamma distributions.
- To obtain each $\pi_l^{(i)}$, $l = 1, \dots, V(V-1)/2$, $i = 1, \dots, n$ simply apply equation (2) to the posterior samples of $Y^{(i)}$, for each $i = 1, \dots, n$ and Z_l , $l = 1, \dots, V(V-1)/2$.
- Impute missing edges $\mathcal{L}(A_i)_l$ from $\mathcal{L}(A_i)_l | \pi_l^{(i)} \sim \text{Bern}\{\pi_l^{(i)}\}$.

Obtaining posterior samples for the subject-specific edge probabilities associated to missing edges is a key for prediction. Under our Bayesian procedure and recalling equation (1), prediction of unobserved edges can be obtained by exploiting the mean of the posterior predictive distribution

$$\begin{aligned} E\{\mathcal{L}(A_i)_l | \mathcal{L}(A_1), \dots, \mathcal{L}(A_n)\} \\ = E\{E\{\mathcal{L}(A_i)_l | \pi_l^{(i)}\} | \mathcal{L}(A_1), \dots, \mathcal{L}(A_n)\} \\ = E\{\pi_l^{(i)} | \mathcal{L}(A_1), \dots, \mathcal{L}(A_n)\}, \quad l = 1, \dots, V(V-1)/2, \end{aligned} \quad (9)$$

for each possible missing edge in subject $i = 1, \dots, n$, where the last expectation coincides with the posterior mean of $\pi_l^{(i)}$. Note that we use standard font $\mathcal{L}(A)$ to define the observed vectors of edges and italics notation $\mathcal{L}(A)$ to denote the associated random variable.

3 Simulation study

We evaluate the performance of our methods on synthetic data simulated from a generating process different than our statistical model. Our goal is to assess whether the proposed methods are sufficiently flexible to learn global and local changes in brain connectivity structures, even when such variations arise from different generative mechanisms.

To accomplish the above goal, we simulate multiple brain networks A_i with $V=20$ nodes and having predictors x_i observed on a discrete grid $x_i \in \mathbb{X} = \{1, \dots, 15\}$. In particular, for each unique predictor value, four networks A_i are generated, for a total of $n=60$

subjects. To imitate the hemispheres and lobes in the brain, we define four node blocks $\mathbb{V}_{L_1} = \{1, \dots, 5\}$, $\mathbb{V}_{L_2} = \{6, \dots, 10\}$, $\mathbb{V}_{R_1} = \{11, \dots, 15\}$ and $\mathbb{V}_{R_2} = \{16, \dots, 20\}$. Nodes in \mathbb{V}_{L_1} and \mathbb{V}_{R_1} belong to the first lobe in the left and right hemisphere, respectively, whereas nodes in \mathbb{V}_{L_2} and \mathbb{V}_{R_2} belong to the second lobe in the left and right hemisphere, respectively.

In simulating the data A_i , we aim to incorporate different topological properties typically observed in human brain networks—covering block-structures by hemispheres and lobes, along with small-world architectures (e.g. Bullmore and Sporns, 2009). In particular, for each unique predictor value in $\mathbb{X}_1 = \{1, \dots, 5\}$, half of the subjects have high assortativity by hemisphere, whereas the others have brains with high lobe assortativity (in this context, the assortativity measures if nodes in the same block are more likely to be connected than nodes in different blocks). Subjects with an intermediate predictor value $x_i \in \mathbb{X}_2 = \{6, \dots, 10\}$ are characterized by brain networks having small-world behavior according to the Watts and Strogatz (1998) model. Finally—consistent with initial descriptive analyses of our data—we increase the interhemispheric density and reduce the intrahemispheric connectivity in the brain networks of the subjects with high predictor value $x_i \in \mathbb{X}_3 = \{11, \dots, 15\}$. As shown in Figure 3 this construction represents a challenging scenario characterized by different network architectures not generated from our model, and changing across the predictors' values with varying patterns of smoothness and subject-specific variability.

To highlight the possible benefits provided by our statistical model, we compare performance with a massive univariate approach estimating a flexible logistic regression for each pair of nodes as follows

$$\mathcal{L}(A_i)_l | \pi_l(x_i) \sim \text{Bern}\{\pi_l(x_i)\}, \quad \text{logit}\{\pi_l(\cdot)\} \sim \text{GP}(\bar{\mu}, \bar{\sigma}c), \quad (10)$$

for $l = 1, \dots, V(V-1)/2$, where c is the correlation function discussed in Section 2, $\bar{\mu}$ is the mean function and $\bar{\sigma}$ is a scaling parameter controlling variability. To borrow information across edges, we set $\bar{\mu}$ equal to the log-odds of the empirical edge probabilities computed for each predictor value in \mathbb{X} and let $\bar{\sigma} = 10$ to allow flexible deviations in each edge trajectory. Posterior inference under the statistical model in equation (10) can be easily performed leveraging the R package BayesLogit.

In performing posterior computation under our model we let $\mu_z = 0$, $\sigma_z^2 = 10$, $a = q = 2$, $\kappa = 0.01$ and set the upper bounds for the latent dimensions at $R = K = 5$. We consider 5000 Gibbs iterations with a burn-in of 1000 and thin the chains every 4 samples—after burn-in. These choices provide good settings for convergence and mixing based on the inspection of the trace-plots for the subject-specific edge probabilities. Posterior computation for our model takes ~ 16 min under a naive R (version 3.2.1) implementation in a

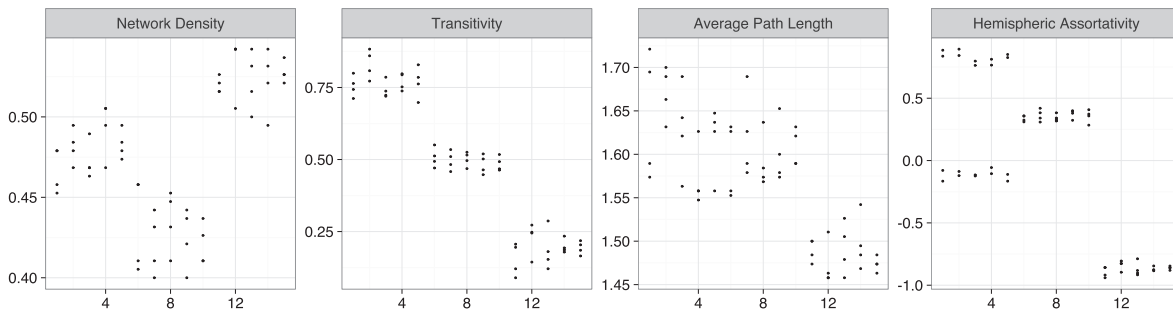


Fig. 3. Scatterplots of the network summary measures computed for the simulated networks A_i , $i = 1, \dots, n$ versus their corresponding predictor value x_i , $i = 1, \dots, n$

machine with 8 Intel Core i7 3.4 GHz processor and 16 GB of RAM. Hence, there are substantial margins to reduce computational time. We consider the same MCMC settings when performing posterior inference for the model in (10), obtaining comparable results for convergence and mixing.

3.1 Inference and predictive performance

The simulated dataset provides a challenging scenario to assess robustness of our methods to model misspecification. We answer this question via posterior predictive checks (Gelman *et al.*, 2014) assessing the flexibility of our formulation in characterizing the network summary measures in Figure 3—of particular interest in neuroscience (Bullmore and Sporns, 2009). Calculation of the posterior predictive distributions for these measures is straightforward using the posterior samples of $\pi_l^{(i)}$, $l = 1, \dots, V(V-1)/2$, $i = 1, \dots, n$, and equation (1).

Figure 4 compares the network summary measures computed from the simulated data with their posterior predictive distribution arising from our network–response regression model and the non-parametric massive univariate logistic regressions in (10), respectively. The closer the points in Figure 4 are to the dashed diagonal line, the better the model characterizes the data. According to results in Figure 4, our formulation achieves general good performance in characterizing the observed networks, even though these data are not generated from a model similar to that described in Section 2. Differently from our flexible network–response regression, the massive univariate logistic regressions fail to carefully incorporate network structure and subject-specific variability, obtaining worse performance.

Although the substantial dimensionality reduction induced by our low-dimensional factorizations in (2) and (5) provide reassurance against over-fitting issues, we empirically assess this property via out-of-sample edge prediction. In accomplishing this goal, we perform posterior computation under both models holding out, for two networks—out of four—in each unique predictor value, those

hard-to-predict edges characterized by more evident variability across subjects. For these held-out data—comprising the 28% of the total number of edges in A_i —we measure out-of-sample predictive performance via the area under the ROC curve (AUC), computed by predicting the edges with the posterior mean of their corresponding edge probabilities estimated from the training data according to equation (9). Explicitly incorporating network structure in modeling of each A_i , while accounting for subject-specific variability, allows us to obtain also accurate out-of-sample inference with an AUC equal to 0.91. When performing prediction under the massive univariate logistic regressions in (10) we obtain a lower AUC equal to 0.82. These results confirm the usefulness of our model as a general and flexible procedure to provide accurate inference on global and local changes in brain networks across traits of interest.

4 Brain networks and intelligence scores

We apply our model to the dataset MRN-114, which consists of brain structural connectivity data for $n = 114$ subjects along with their cognitive ability measured via FSIQ score (Jung and Haier, 2007). This score ranges from 86 to 144 with 48 unique values observed in our data. In studying the association between intelligence and brain architecture, previous works either focus on detecting the activated brain regions in cognitive control (e.g. Leech *et al.*, 2012) or study relationships between intelligence and topological network measures (e.g. Li *et al.*, 2009). We hope to obtain new insights into the neural pathways underlying human intelligence.

In performing posterior computation we consider a total of 5000 Gibbs samples, setting $\mu_z = 0$, $\sigma_z^2 = 10$, $a = q = 2$, and $\kappa = 0.001$. In this case the algorithm required ~ 3.5 h. As in the simulation study, trace-plots for the edge probabilities suggest that convergence is reached after 1000 burn-in iterations. We additionally thin the chain by collecting every 4 samples. Since the latent dimensions R and K are unknown, we perform posterior computation for increasing $R = K = 1, \dots, 6$ and stop when there is no substantial

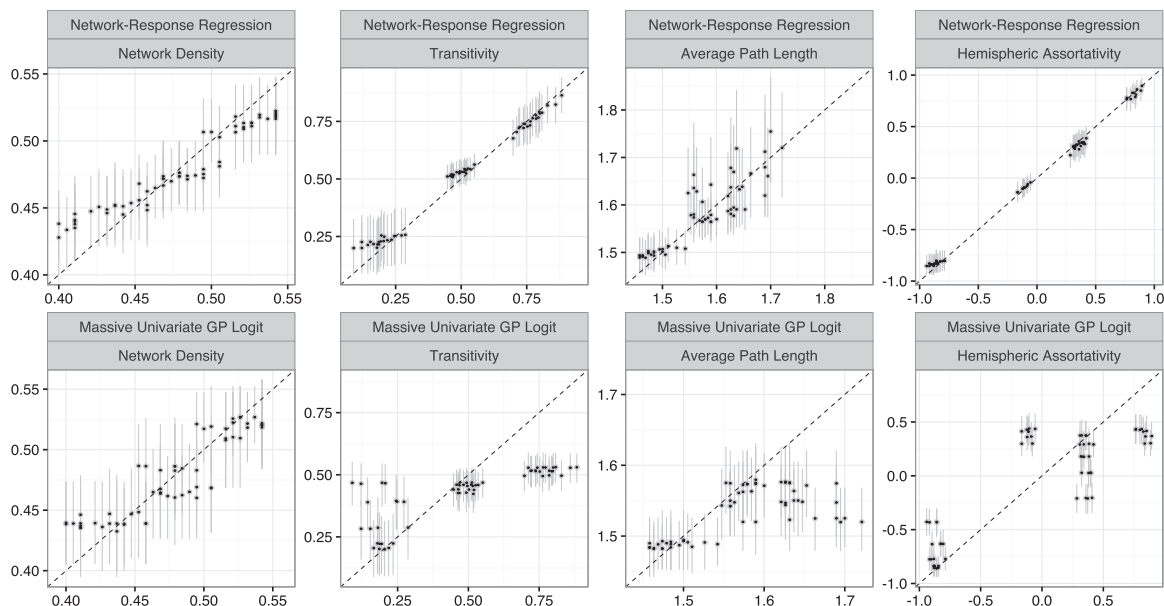


Fig. 4. Goodness-of-fit assessment for selected network summary measures under the two different modeling procedures in the simulation study. Upper panels: for the Bayesian network–response regression, plot of the network summary measures computed from the simulated subjects (x-axis) versus their corresponding mean arising from the posterior predictive distribution (y-axis). Segments represent the 95% posterior predictive intervals. Lower panels: same quantities from the massive univariate nonparametric logistic regression

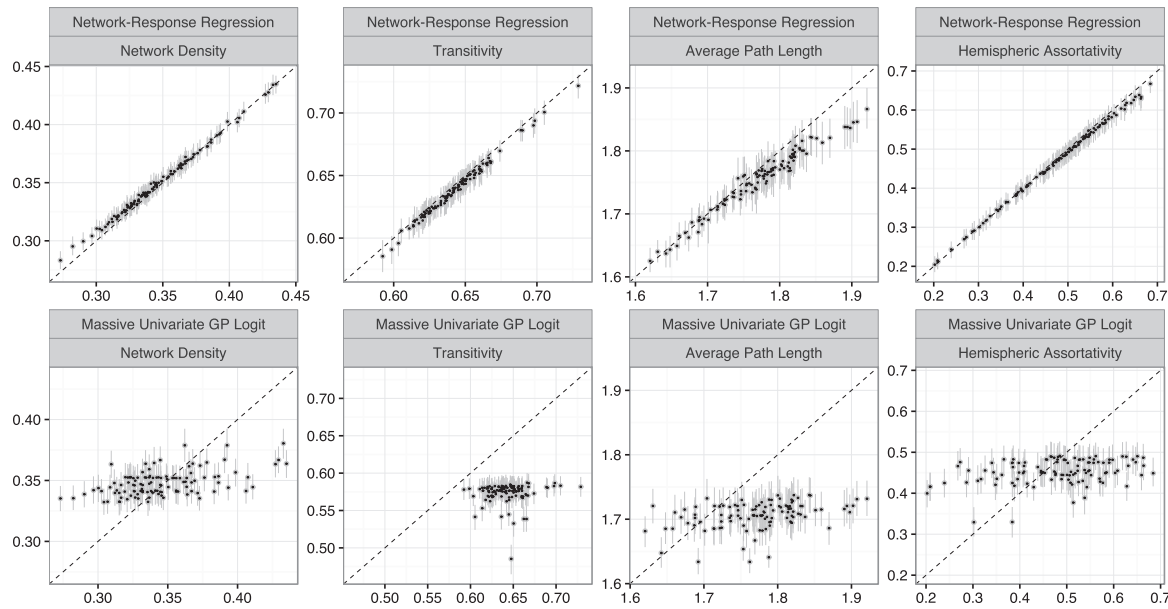


Fig. 5. Goodness-of-fit assessment for selected network summary measures under the two different modeling procedures in the application. Upper panels: for the Bayesian network–response regression, plot of the network summary measures computed from the observed subjects (x-axis) versus their corresponding mean arising from the posterior predictive distribution (y-axis). Segments represent the 95% posterior predictive intervals. Lower panels: same quantities from the massive univariate nonparametric logistic regression

Table 1. Average AUC computed for the test data at varying R and K

$R = K = 1$	$R = K = 2$	$R = K = 3$	$R = K = 4$	$R = K = 5$	$R = K = 6$
0.983	0.986	0.988	0.989	0.990	0.989

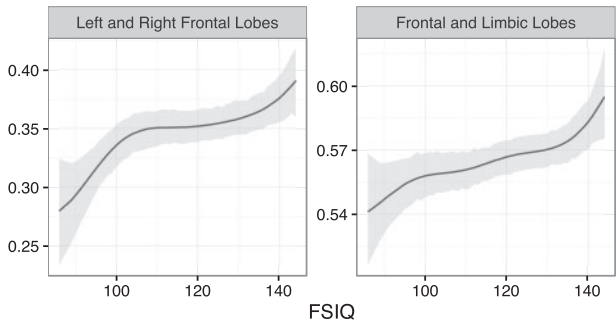


Fig. 6. Left plot: average edge probability versus FSIQ for connections linking regions in left and right frontal lobe. Right plot: average edge probability versus FSIQ for connections linking regions in frontal and limbic lobes. Black lines denote the point-wise posterior means and gray areas denote the 95% highest posterior density intervals from our model

improvement in out-of-sample edge prediction based on the AUC. In computing the AUC, we randomly select 20% of the edges and hold them out for a randomly chosen 50% of the subjects. For these held-out test edges, the AUC is computed as discussed in the simulation. We repeat the procedure 5 times for each setting and report the average AUC in Table 1. The network-response model having $R = K = 5$ provides a good choice for inference and prediction. It is additionally worth noticing how all the AUCs are very high. The reason for this result is that a wide set of brain connections are easier to predict in being either almost always present or absent in the subjects under study.

In the following subsections we discuss the improved performance of our procedure—considering $R = K = 5$ —in relation to our

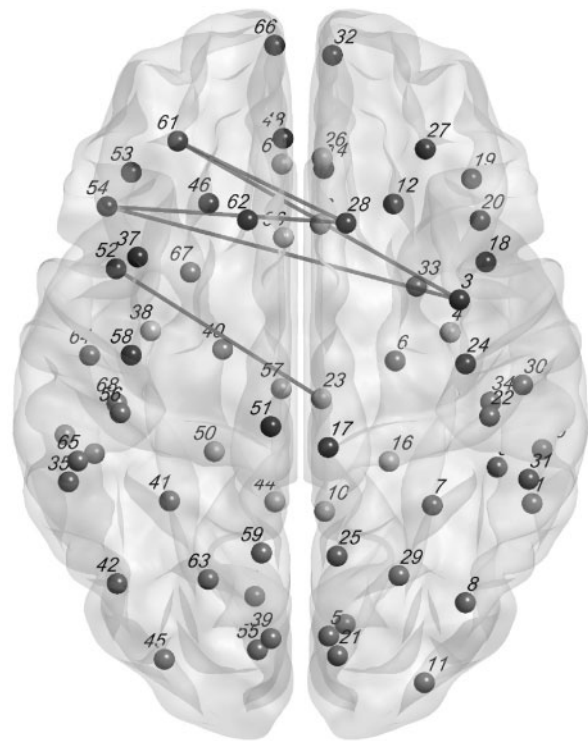


Fig. 7. 3-D brain network representation showing edges whose trajectories display evident trends across FSIQ—based on their posterior distributions. Brain regions having the same shade of gray belong to the same anatomical lobe

Table 2. Proportion of actual edges among those predicted to have an edge with probability within each bin

	[0, 0.1]	(0.1, 0.2]	(0.2, 0.3]	(0.3, 0.4]	(0.4, 0.5]	(0.5, 0.6]	(0.6, 0.7]	(0.7, 0.8]	(0.8, 0.9]	(0.9, 1]
Bayesian network–response regression	0.07	0.16	0.23	0.34	0.42	0.53	0.62	0.70	0.80	0.91
Massive univariate GP logistic regression	0.23	0.27	0.33	0.39	0.45	0.50	0.59	0.62	0.63	0.70

competitor in (10), including in inference, prediction and uncertainty quantification. These relevant improvements are fundamental in refining inference on how network structures change across a continuous trait of interest.

4.1 Goodness-of-fit and inference on changes in the brain connectivity architecture across FSIQ scores

As discussed in Sections 1 and 3, restrictive statistical models for how a brain network architecture changes with a trait can lead to substantially biased inference and conclusions. Hence, prior to presenting our findings, we first assess the performance of our statistical model in characterizing the observed brain network data. Consistent with the analyses in Section 3, this is accomplished via posterior predictive checks for relevant topological properties. As shown in Figure 5, our model achieves good performance in characterizing the observed network summary measures, substantially improving over our competitor. This motivates further analyses on how the brain network changes, on average, across FSIQ scores.

The cerebrum of the brain is divided into five main anatomical lobes—named frontal, limbic, occipital, parietal and temporal lobes (Kang *et al.*, 2012). In order to provide interpretable inference on how the network structure changes with FSIQ, we focus on the posterior distribution for the trajectories of aggregated connectivity patterns considering possible combinations of hemispheric and lobe membership. For example, the left plot in Figure 6 displays the posterior distribution of the averaged edge probabilities connecting brain regions in different hemispheres, but belonging both to the frontal lobe.

Figure 6 shows that the aggregated pathway linking regions in the left and right frontal lobe, as well as the one connecting regions in the frontal lobe with those in the limbic cortex, increase with FSIQ. This result is in line with findings on the role of the frontal lobe in intelligence (Li *et al.*, 2009). To provide insights on local changes in the brain architecture with FSIQ, Figure 7 highlights the connections whose posterior distributions show evident trends with FSIQ. In particular all the trajectories for the edges highlighted in Figure 7 significantly increase with FSIQ. Consistent with the results in the left plot of Figure 6, almost all these edges connect regions in opposite hemispheres but belonging both to the frontal lobe.

4.2 Edge prediction and uncertainty quantification

Results in Figure 5 are appealing in demonstrating that the substantial dimensionality reduction induced by our model via (2) and (5), carefully preserves flexibility in characterizing complex brain network structures and their changes with FSIQ. To further investigate the benefits induced by our parsimonious representation we assess performance in edge prediction for a challenging scenario holding out—for 50% of the subjects—only the hard-to-predict edges having empirical probability (the empirical edge probability $\bar{\pi}_l$ is defined as $\bar{\pi}_l = \sum_{i=1}^n \mathcal{L}(A_i)_l / n$ for each $l = 1, \dots, V(V-1)/2$) $0.2 < \bar{\pi}_l < 0.8$. Consistent with the results in the simulation study we obtain an AUC equal to 0.82, substantially out-performing the AUC of 0.65 for our competitor.

Another advantage of our flexible Bayesian approach over methods relying on optimization or restrictive hierarchical models is the ability to accurately characterize uncertainty in learning how the brain structure varies with subjects, systematically in relation to a trait and randomly due to unobserved conditions or measurement errors. We assess performance in uncertainty quantification by evaluating probability calibration in the above prediction task. In particular, we bin the estimated probabilities for the held-out edges in intervals $[0, 0.1], (0.1, 0.2], \dots, (0.9, 1]$ and—within each bin—we calculate the proportion of actual edges among those predicted to have an edge probability within that bin. If the values of these empirical proportions are actually within the bins they refer to, the procedure is well calibrated and properly quantifies uncertainty. According to Table 2 our model has good performance in uncertainty quantification.

5 Conclusion

Motivated by a neuroscience study, we developed a novel model to flexibly infer changes in a network-valued random variable with a continuous trait. The simulation study and the application to learn variations in the brain connectivity architecture across FSIQ show substantial improvements in inference, edge prediction and uncertainty quantification.

Although we focus on a single trait, the method is trivially generalized to accommodate multiple traits of an individual. Moreover our formulation can be easily adapted to incorporate directed networks via two subsets of latent coordinates—for each brain region—modeling outgoing and incoming edges, respectively. Our procedure also has a broad range of possible applications in social science and econometrics.

Although our initial results suggest that binary brain networks already contain valuable information about the individual’s brain structure, future research generalizing the proposed model to account for weighted edges, may benefit from the additional information contained in the fiber counts.

Acknowledgements

We thank Joshua T. Vogelstein for getting us interested in statistical and computational methods for analysis of brain networks. We are also grateful to the Associate Editor and the referees for their valuable comments on a first version of this manuscript.

Funding

This work was partially supported by the grant N00014-14-1-0245 of the United States Office of Naval Research (ONR), and grant CPDA154381/15 of the University of Padova, Italy.

Conflict of Interest: none declared.

References

Airolidi, E.M. *et al.* (2008) Mixed membership stochastic blockmodels. *J. Mach. Learn. Res.*, 9, 1981–2014.

- Bullmore, E. and Sporns, O. (2009) Complex brain networks: graph theoretical analysis of structural and functional systems. *Nat. Rev. Neurosci.*, **10**, 186–198.
- Desikan, R.S. et al. (2006) An automated labeling system for subdividing the human cerebral cortex on MRI scans into gyral based regions of interest. *Neuroimage*, **31**, 968–980.
- Durante, D. and Dunson, D.B. (2014) Nonparametric Bayes dynamic modeling of relational data. *Biometrika*, **101**, 883–898.
- Frank, O. and Strauss, D. (1986) Markov graphs. *J. Am. Stat. Assoc.*, **81**, 832–842.
- Gelman, A. et al. (2014) *Bayesian Data Analysis*. Taylor & Francis, Boca Raton, FL.
- Hochberg, Y.V. et al. (2007) Whom you know matters: venture capital networks and investment performance. *J. Finance*, **62**, 251–301.
- Hoff, P.D. (2008) Modeling homophily and stochastic equivalence in symmetric relational data. In: Platt, J. et al. (ed.) *Advances in Neural Information Processing Systems 20*. MIT Press, Cambridge, MA, pp. 657–664.
- Hoff, P.D. et al. (2002) Latent space approaches to social network analysis. *J. Am. Stat. Assoc.*, **97**, 1090–1098.
- Holland, P.W. and Leinhardt, S. (1977) A dynamic model for social networks. *J. Math. Sociol.*, **5**, 5–20.
- Jung, R.E. and Haier, R.J. (2007) The parieto-frontal integration theory (P-FIT) of intelligence: converging neuroimaging evidence. *Behav. Brain Sci.*, **30**, 135–154.
- Kang, X. et al. (2012) Hemispherically-unified surface maps of human cerebral cortex: reliability and hemispheric asymmetries. *PLoS ONE*, **7**, e45582.
- Leech, R. et al. (2012) Echoes of the brain within the posterior cingulate cortex. *J. Neurosci.*, **32**, 215–222.
- Li, Y. et al. (2009) Brain anatomical network and intelligence. *PLoS Comput. Biol.*, **5**, e1000395.
- Mueller, S. et al. (2013) Individual variability in functional connectivity architecture of the human brain. *Neuron*, **77**, 586–595.
- Nowicki, K. and Snijders, T.A.B. (2001) Estimation and prediction for stochastic blockstructures. *J. Am. Stat. Assoc.*, **96**, 1077–1087.
- O'Malley, A.J. and Marsden, P.V. (2008) The analysis of social networks. *Health Serv. Outcomes Res. Methodol.*, **8**, 222–269.
- Polson, N.G. et al. (2013) Bayesian inference for logistic models using Pólya–Gamma latent variables. *J. Am. Stat. Assoc.*, **108**, 1339–1349.
- Rubinov, M. and Sporns, O. (2010) Complex network measures of brain connectivity: uses and interpretations. *Neuroimage*, **52**, 1059–1069.
- Sewell, D.K. and Chen, Y. (2015) Latent space models for dynamic networks. *J. Am. Stat. Assoc.*, **110**, 1646–1657.
- Simpson, S.L. et al. (2013) Analyzing complex functional brain networks: fusing statistics and network science to understand the brain. *Stat. Surv.*, **7**, 1–36.
- Stam, C.J. (2014) Modern network science of neurological disorders. *Nat. Rev. Neurosci.*, **15**, 683–695.
- van den Heuvel, M.P. et al. (2009) Efficiency of functional brain networks and intellectual performance. *J. Neurosci.*, **29**, 7619–7624.
- Watts, D.J. and Strogatz, S.H. (1998) Collective dynamics of small-world networks. *Nature*, **393**, 440–442.
- Wu, K. et al. (2013) A longitudinal study of structural brain network changes with normal aging. *Front. Hum. Neurosci.*, **7**, 113.
- Xing, E.P. et al. (2010) A state-space mixed membership blockmodel for dynamic network tomography. *Ann. Appl. Stat.*, **4**, 535–566.